WARSAW UNIVERSITY OF TECHNOLOGY Index 351733
FACULTY OF CIVIL ENGINEERING
COMMITTEE FOR CIVIL AND WATER ENGINEERING
POLISH ACADEMY OF SCIENCES ISSN 1230-2945
DOI: 10.24425/ace.2025.155098
ARCHIVES OF CIVIL ENGINEERING
Vol. LXXI ISSUE 3 2025
pp. 265 –279

Research paper

Study on seismic performance of aeolian sand concrete shear walls with CFST columns and concealed bracings

Yaohong Wang[1], Zezhou Su[2]

Abstract: In order to promote the application of aeolian sand resources in steel-concrete composite shear wall, a kind of aeolian sand concrete shear walls with concrete filled steel tube (CFST) columns and concealed bracings is proposed in this paper. The shear wall is composed of aeolian sand concrete, steel bar, steel tube and steel plate. Through the low cyclic loading test of three aeolian sand concrete shear walls with CFST columns specimens and aeolian sand concrete shear walls with CFST columns and concealed bracings specimens, the influence mechanism of setting concealed bracing on the seismic performance of the specimens was revealed. The results show that under the same replacement rate of aeolian sand, the setting of concealed bracing can significantly improve the load-carrying capacity, ductility, stiffness degradation behavior and energy dissipation capacity of the specimens. In addition, the calculation models of normal section bearing capacity for aeolian sand concrete shear walls with CFST columns and aeolian sand concrete shear walls with CFST columns and concealed bracings are established. The test results are in good agreement with the calculation results.

Keywords: aeolian sand, concealed bracing, load-carrying capacity, shear wall, seismic performance

[1]Prof., PhD., Inner Mongolia University of Technology, College of Civil Engineering, Hohhot, China, e-mail: wyh@imut.edu.cn, ORCID: 0000-0002-6389-9338

[2]MSc., Inner Mongolia University of Technology, College of Civil Engineering, Hohhot, China, e-mail: 20211100315@imut.edu.cn, ORCID: 0009-0002-6058-5293

1. Introduction

In recent years, China's infrastructure construction and urbanization construction have been vigorously developed, and the demand for concrete has increased dramatically. This has not only led to a serious shortage of natural resources such as sand and gravel in China, but also brought serious damage to the natural environment. At the same time, there are a large number of aeolian sand resources in the northwest of China. If aeolian sand can be reasonably applied to building structures, it is of great significance to reduce project cost and protect the ecological environment.

Aeolian sand concrete refers to the concrete prepared by partially replacing river sand with aeolian sand [1]. H.J. Xue, et al. [2] showed that with the increase of aeolian sand content, the compressive strength and splitting tensile strength of concrete cubes increased first and then decreased, and the concrete with aeolian sand content of 20%, 30% and 40% could meet the design strength requirements. W.L. Li [3] conducted in-depth research on the road performance of aeolian sand concrete. X.S. Guo [4] shows that the preparation of aeolian sand concrete by alkali-activated fly ash at room temperature is beneficial to improve its wind erosion resistance, freeze-thaw resistance and wind erosion-freeze-thaw durability

Steel-concrete composite shear wall has the advantages of high bearing capacity, slow stiffness degradation and good ductility [5]. According to Ref. [6, 7], the seismic performance of concrete filled steel tube (CFST) frame with concealed steel plate composite shear wall is significantly higher than that of ordinary concrete shear wall. According to Ref. [8], the concrete shear wall with concealed bracing has high lateral bearing capacity and energy dissipation capacity. In addition, some scholars have studied the bearing capacity formula of shear wall members [9–11].

At present, there are few studies on steel-aeolian sand concrete composite shear wall in China. In order to promote the application of aeolian sand resources in steel-concrete composite shear walls, this paper designs and manufactures three-sided aeolian sand concrete shear walls with CFST columns and aeolian sand concrete shear walls with CFST columns and concealed bracings, and conducts low-cycle repeated load tests on them. On the basis of experimental research, an analysis model was established to calculate and verify the normal section bearing capacity of the above two shear wall specimens. The variables of the experiment are the replacement rate of aeolian sand to river sand and whether the concealed bracings is set. The purpose of the test is to study the influence mechanism of setting concealed bracings on the seismic performance of specimens under the same replacement rate of aeolian sand.

2. Test program

2.1. Test specimens

A total of three aeolian sand concrete shear walls with CFST columns and concealed bracings were designed. The scale ratio was 1:5. The replacement rates of aeolian sand were 20, 30 and 40%, respectively, and the numbers were TZSW1, TZSW2 and TZSW3. For comparative

study, this paper introduces the experimental data of three aeolian sand concrete shear walls with CFST columns, numbered TSW1, TSW2 and TSW3 respectively. The geometric size, axial compression ratio and reinforcement ratio of each specimen are the same. The shear span ratio of the six shear walls is 1.5, and the wall size is 630 mm × 100 mm × 795 mm (width × thickness × height). The concrete cover thickness of the wall is 10 mm, and the concrete cover thickness of the top beam and the bottom beam is 40 mm. HRB400 steel bars are used in the distribution of steel bars in the wall. The longitudinal reinforcement ratio is 1.87%, and the transverse reinforcement ratio is 1.52%. The U-shaped shear key with a spacing of 198 mm and a diameter of 6 mm is welded on the steel tube to ensure the effective connector between the CFST frame and the wall panel [9]. For the specimens TZSW1, TZSW2 and TZSW3, a steel plate with a width of 70 mm and a thickness of 6 mm was placed in the wall as a concealed bracings, and extended to the top beam and the bottom beam to be welded together with the steel tube. The basic design parameters of each specimen are shown in Table 1, and the dimensions and reinforcement details are shown in Fig. 1. The mixture ratio of concrete is shown in Table 2. Three 150 mm × 150 mm × 150 mm test cube were made for each concrete, and the cube compressive strength test was carried out after 28 days of curing. The mechanical properties of steel are shown in Table 3.

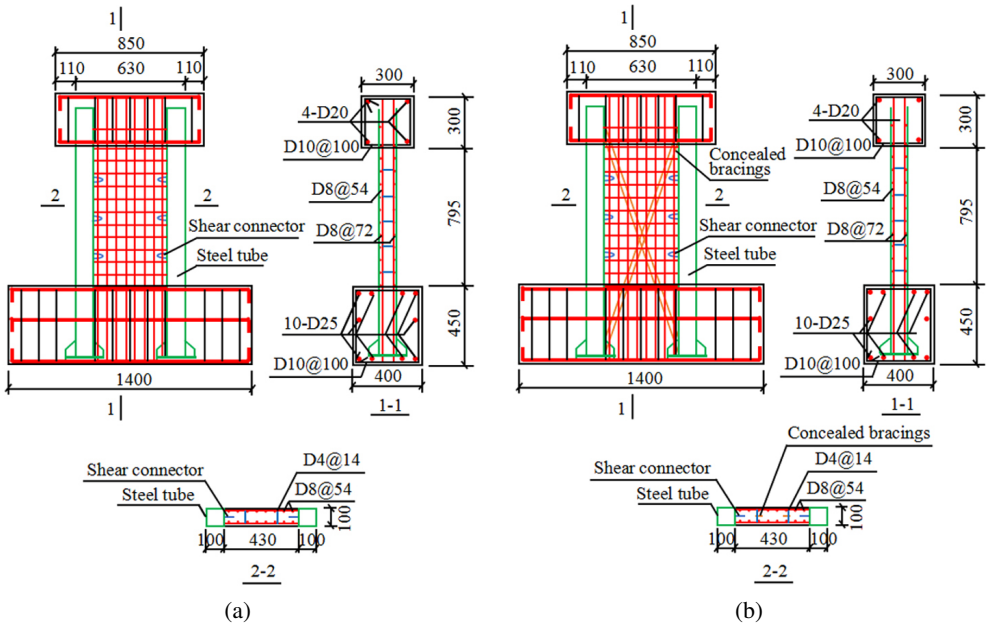

Fig. 1. Dimensions and reinforcement details of specimens (units: mm): (a) Vertical view of specimen TSW1 ~ TSW3, (b) Vertical view of specimen TZSW1 ~ TZSW3

Table 1. Design parameters of the specimens

Specimen number	Concrete strength grade	Aeolian sand replacement ratio β (%)	Shear span ratio	Axial compression ratio	Concealed bracings
TSW1	C35	20	1.5	0.2	No
TSW2	C35	30	1.5	0.2	No
TSW3	C35	40	1.5	0.2	No
TZSW1	C35	20	1.5	0.2	Yes
TZSW2	C35	30	1.5	0.2	Yes
TZSW3	C35	40	1.5	0.2	Yes

Table 2. Mixture ratio and mechanical properties of concrete

Aeolian sand replacement rate (%)	Material content (kg·m^{-3})							f_{cu} /MPa	f_c /MPa
	Cement	Coal ash	Water	Stone	River sand	Eolian sand	Water reducer		
20	332	129	185	923	665	166	0.461	41.2	27.60
30	332	129	185	923	582	249	0.461	45.2	30.28
40	332	129	185	923	499	332	0.461	43.6	29.21
Note: f_{cu} and f_c are the cubic compressive strength and axial compressive strength of concrete, respectively. The relationship between f_{cu} and f_c is as follows: $f_c = \alpha f_{cu}$ [12].									

Table 3. Mechanical properties of steel materials

Steel type	Thicknes (mm)	Grade	f_y (MPa)	f_u (MPa)	E_s ($\times 10^5$ MPa)
D8 distributing bar	–	HRB400	426.4	533.7	2.02
Steel shear connector	6	HRB400	412.5	542.6	2.00
Steel tube	4	Q235	273.8	406.3	2.03
Steel plate	6	Q235	278.2	405.5	2.09
Note: f_y, f_u and E_s are the yield stress, ultimate stress and elastic modulus of steel respectively.					

2.2. Loading and testing procedures

The specimens were tested under horizontal low cyclic loading and constant axial load. The test loading device is shown in Fig. 2. The axial compression ratio of the six-sided shear wall specimens is 0.2, and the axial pressure is 175 kN. When loading, the constant axial load is first applied by a hydraulic jack with a limit capacity of 1000 kN, and then the horizontal cyclic load is transferred to the center of the loading beam by an electro-hydraulic servo actuator

with a capacity of 500 kN. Displacement meters are arranged in the middle of the top beam, the bottom beam and the wall. The loading scheme of the load and displacement mixed control was adopted. Before the specimen yields, the load control grading loading is adopted, and the load increment of each stage is an integer multiple of 10 kN, and each stage load is cycled once. After the specimen yields, the load control is changed to displacement control. The displacement Δ is controlled to be an integer multiple of the yield displacement Δ_y, and each stage of displacement is cycled once until the load drops below 85% of the peak load.

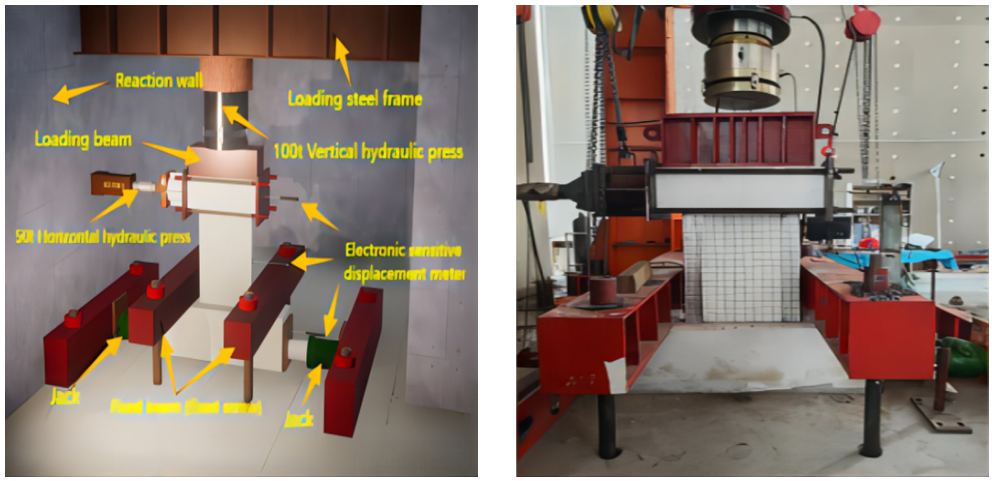

(a) (b)

Fig. 2. Test setup: (a) Schematic diagram, (b) Photograph

3. Results and discussion

3.1. Failure modes

The final failure modes of the six specimens are shown in Fig. 3. Figure 4 show the local failure diagram of TSW2 and TZSW2. The failure characteristics of each shear wall have the following characteristics:

1. The crack distribution of aeolian sand concrete shear walls with CFST columns is relatively evacuated. The initial crack appears at the interface between the frame and the wall, and develops obliquely downward 45°. In the middle stage of loading, oblique downward cross cracks increase. In the later stage of loading, slight bulging occurred at the bottom of the steel tubes on both sides of the specimen (Fig. 4a), and concrete spalling occurred at the bottom of the junction between the steel tube and the wallboard.
2. The crack distribution of aeolian sand concrete shear walls with CFST columns and concealed bracings is dense, and the development direction of oblique crack tends to the angle between concealed bracing and horizontal line. In the later stage of loading, slight

bulging and paint flakes fall off at the bottom of the steel tubes on both sides of the specimen (Fig. 4b), and different degrees of concrete spalling occur at the intersection of the concealed bracings, that is, the shear compression zone, which is also an important reason for the increase of energy dissipation capacity of the aeolian sand concrete shear walls with CFST columns and concealed bracings.

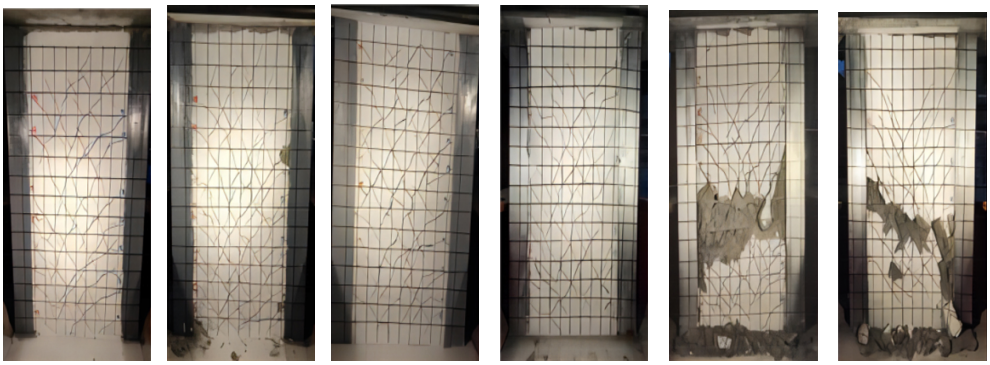

(a) (b) (c) (d) (e) (f)

Fig. 3. Failure modes of specimens: (a) TSW1, (b) TSW2, (c) TSW3, (d) TZSW1, (e) TZSW2, (f) TZSW3

(a) (b)

Fig. 4. Local damage modes of specimens: (a) TSW2, (b) TZSW2

3.2. Hysteresis curves

Figure 5 shows the load – displacement (F–Δ) hysteresis curve of each specimen under low cyclic loading. From Fig. 5, it can be seen that when the replacement rate of aeolian sand is the same, the hysteresis loop of specimen TZSW1 ~ TZSW3 is fuller and the middle pinching is lighter than that of specimen TSW1 ~ TSW3, which shows that the setting of concealed bracings can significantly improve the energy dissipation capacity of aeolian sand concrete shear walls with CFST columns and concealed bracings; In the specimens TZSW1 ~ TZSW3, when the replacement rate of aeolian sand increases from 20% to 30%, the hysteresis loop of

the specimen becomes fuller, and when the replacement rate of aeolian sand increases from 30% to 40%, the hysteresis loop of the specimen shows a pinching trend, indicating that the energy dissipation capacity of the aeolian sand concrete shear walls with CFST columns and concealed bracings with 30% replacement rate of aeolian sand is higher. This is because the tensile strength of aeolian sand concrete with an aeolian sand replacement rate of 30% is higher, which makes the concrete of the shear wall specimen in the tensile zone more difficult to crack, thereby improving the energy dissipation capacity of the shear wall specimen [2].

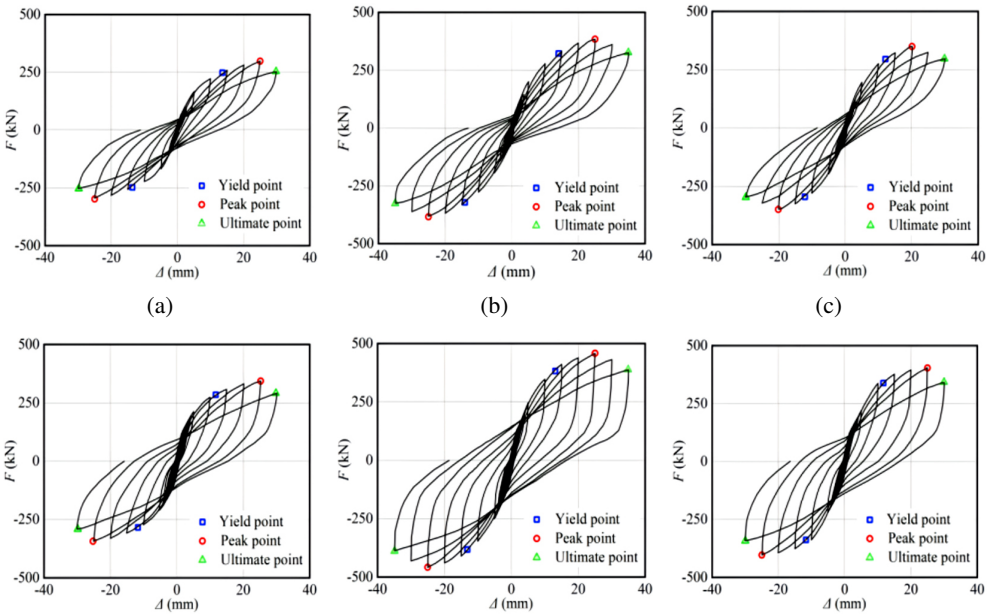

Fig. 5. Hysteretic curves: (a) TSW1, (b) TSW2, (c) TSW3, (d) TZSW1, (e) TZSW2, (f) TZSW3

3.3. Skeleton curves

Figure 6 show the load-displacement (F–Δ) skeleton curve of each specimen obtained from the test. Table 4 shows the load and displacement of each shear wall specimen at the characteristic points of cracking, yield, peak and ultimate. In the table: the load and displacement of each characteristic point take the average of the load and displacement in the positive and negative directions; the cracking point is defined as the point corresponding to the first loading cracking; the yield point is calculated by the energy equivalent method [10]; the peak point is defined as the maximum horizontal load point; the ultimate point is defined as the point when the load drops to 85% of the peak load. The ductility coefficient μ is defined as the ratio of $\Delta_{u,t}$ to $\Delta_{y,t}$, which is used to measure the ductility of the component.

The result from Fig. 6 and Table 4 show the following:

Table 4. Load and displacement of characteristic points of specimens

Specimen	Cracking point		Yield point		Peak point		Ultimate point		μ
	$F_{c,t}$ /kN	$\Delta_{c,t}$ /mm	$F_{y,t}$ /kN	$\Delta_{y,t}$ /mm	$F_{p,t}$ /kN	$\Delta_{p,t}$ /mm	$F_{u,t}$ /kN	$\Delta_{u,t}$ /mm	
TSW1	99.83	2.72	248.16	13.58	298.29	25.01	253.63	29.81	2.20
TSW2	99.92	2.04	321.69	13.64	383.97	24.98	326.41	34.97	2.56
TSW3	99.87	2.42	295.34	13.11	349.41	20.10	297.32	29.86	2.28
TZSW1	100.11	1.81	284.13	11.71	343.28	25.25	291.26	29.83	2.54
TZSW2	100.34	1.54	382.32	13.15	458.09	25.02	388.76	34.92	2.66
TZSW3	100.27	1.70	338.04	11.68	403.48	24.98	342.51	29.96	2.57

1. The peak load of specimens TZSW1 ~ TZSW3 is greater than that of specimens TSW1 ~ TSW3 under the same aeolian sand replacement rate.
2. Compared with specimen TSW1, the yield and peak load of specimen TZSW1 increased by 14.49% and 15.08% respectively. Compared with specimen TSW2, the yield and peak load of specimen TZSW2 increased by 18.85% and 19.30% respectively. Compared with specimen TSW3, the yield and peak load of specimen TZSW3 increased by 14.46% and 15.47% respectively.
3. The ductility factor of specimen TZSW1 is 15.45% higher than that of specimen TSW1, the ductility factor of specimen TZSW2 is 3.91% higher than that of specimen TSW2, and the ductility factor of specimen TZSW3 is 12.72% higher than that of specimen TSW3.
4. In the specimens TZSW1 ~ TZSW3, when the replacement rate of aeolian sand increased from 20% to 30%, the yield load, peak load and ductility factor of the specimens increased by 34.56%, 33.45% and 4.72%, respectively. When the replacement rate of aeolian sand increased from 30% to 40%, the yield load, peak load and ductility factor of the specimens decreased by 11.58%, 11.92% and 3.38%, respectively.

The above analysis show that under the same replacement rate of aeolian sand, the setting of concealed bracings can improve the load-carrying capacity and ductility of the aeolian sand concrete shear walls with CFST columns and concealed bracings, and when the replacement rate of aeolian sand is 30%, the shear wall have higher load-carrying capacity and better ductility.

3.4. Degradations of stiffness

The secant stiffness is used to represent the stiffness degradation characteristics of the specimen under horizontal low cyclic loading. The secant stiffness K_i is calculated as follows [11]:

$$K_i = \frac{\left|F_i^+\right| + \left|F_i^-\right|}{\left|\Delta_i^+ + \Delta_i^-\right|} \tag{3.1}$$

where: F_i^+ and F_i^- are the maximum loads in the positive and negative directions at the ith cycle, respectively; Δ_i^+ and Δ_i^- are the lateral displacements corresponding to F_i^+ and F_i^-, respectively.

The measured values of the stiffness of each specimen and the stiffness attenuation coefficient of each stage are shown in Table 5. Where: K_0 is the initial elastic stiffness, which is defined as the stiffness of the specimen in the linear elastic stage; K_c is the cracking secant stiffness of the specimen; K_y is the yield secant stiffness of the specimen; $\beta_{c0} = K_c/K_0$ is the stiffness attenuation coefficient of the specimen from the initial elasticity to the cracking process; $\beta_{y0} = K_y/K_0$ is the stiffness attenuation coefficient of the specimen from initial elasticity to yield. Figure 7 show the measured curve of the stiffness K of each shear wall decreasing with the increase of the displacement angle θ.

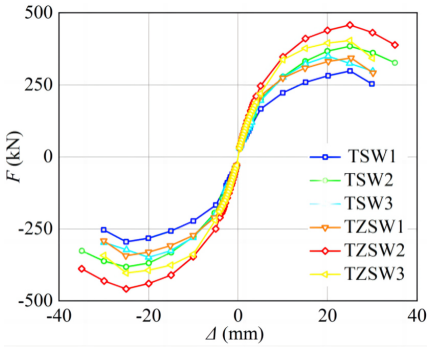

Fig. 6. Skeleton curves

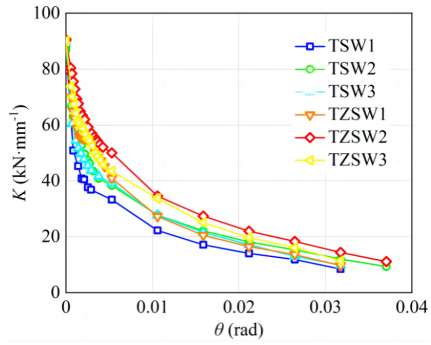

Fig. 7. Stiffness degradation curves

The results from Fig. 7 and Table 5 show the following:

1. The stiffness degradation curve of specimen TZSW1 ~ TZSW3 is more moderate than that of specimen TSW1 ~ TSW3.
2. The K_0 and K_y values of specimen TZSW1 are 50.71% and 32.79% higher than those of specimen TSW1. The K_0 and K_y values of TZSW2 are 33.03% and 23.28% higher than those of TSW2. The K_0 and K_y values of TZSW3 are 42.91% and 28.45% higher than those of TSW3.
3. The β_{co} and β_{y0} values of the specimen TZSW1 are 47.62% and 28.57% higher than those of the specimen TSW1. The β_{co} and β_{y0} values of specimen TZSW2 are 30.36% and 22.22% higher than those of specimen TSW2. The β_{co} and β_{y0} values of specimen TZSW3 are 41.30% and 28.00% higher than those of specimen TSW3.
4. In the specimens TZSW1 ~ TZSW3, when the replacement rate of aeolian sand increased from 20% to 30%, the β_{co} and β_{y0} values of the specimens increased by 17.74% and 22.22%, respectively. When the replacement rate of aeolian sand increased from 30% to 40%, the β_{co} and β_{y0} values of the specimens decreased by 10.96% and 3.03%, respectively.

The above analysis show that under the same replacement rate of aeolian sand, the setting of concealed bracings can effectively slow down the stiffness attenuation rate of aeolian sand concrete shear walls with CFST columns and concealed bracings. This is because concealed bracings can form reinforced concrete core bundles in the wallboard and restrain the development of concrete cracks, so that the stiffness and performance of the specimens are relatively stable in the later stage [13], and when the aeolian sand replacement rate is 30%, the stiffness of the shear wall decays slowly.

Table 5. Experimental results of stiffness

Specimen	K_0 (kN/mm)	K_c (kN/mm)	K_y (kN/mm)	β_{co}	β_{y0}
TSW1	87.00	36.70	18.27	0.42	0.21
TSW2	87.92	48.98	23.58	0.56	0.27
TSW3	88.81	41.27	22.53	0.46	0.25
TZSW1	89.85	55.31	24.26	0.62	0.27
TZSW2	89.10	65.16	29.07	0.73	0.33
TZSW3	90.14	58.98	28.94	0.65	0.32

3.5. Energe dissipation

The cumulative energy dissipation coefficient E_p and the equivalent viscous damping coefficient ξ_e are important indexes to evaluate the energy dissipation capacity of shear wall specimens. E_p reflects the actual energy dissipation capacity of the structure, and ξ_e reflects the fullness of the hysteresis loop. E_p is defined as the total area of the hysteresis curves of all the first loading cycles under each loading amplitude [14]. The equivalent viscous damping coefficient ξ_e is calculated as follows [15]:

$$\xi_e = \frac{1}{2\pi} \frac{S_{(\mathrm{ABC+CDA})}}{S_{(\mathrm{OBE+ODF})}} \tag{3.2}$$

where: $S_{(\mathrm{ABC+CDA})}$ is the area of the hysteresis curve of the first loading period under each loading amplitude, and $S_{(\mathrm{OBE+ODF})}$ is the sum of the two triangular areas of OBE and ODF under the same loading period, as shown in Fig. 8.

Figure 9 show the cumulative hysteretic energy dissipation curve of the specimen. Figure 10 show the equivalent viscous damping coefficient of the specimen at the characteristic point.

The results from Fig. 9 and Fig. 10 show the following:

1. The stiffness degradation curve of specimens TZSW1 ~ TZSW3 is significantly higher than that of specimens TSW1 ~ TSW3.
2. When the replacement rate of aeolian sand is the same, the ξ_e value of the specimen TZSW1 ~ TZSW3 at the characteristic point is larger than that of the specimen TSW1 ~ TSW3, indicating that the hysteresis loop pinch of the specimen TZSW1 ~ TZSW3 is lighter.
3. In the specimens TZSW1 ~ TZSW3, the ξ_e value of the specimen TZSW2 at the feature point is greater than that of the specimen TZSW1. When the aeolian sand replacement rate is increased to 40%, the ξ_e value of the specimen TZSW3 at the feature point is lower than that of the specimen TZSW2, indicating that the hysteresis loop of the specimen with the aeolian sand replacement rate of 30% is lighter.

The above analysis show that under the same replacement rate of aeolian sand, the setting of concealed bracings can significantly improve the energy dissipation capacity of aeolian sand concrete shear walls with CFST columns and concealed bracings. And when the replacement rate of aeolian sand is 30%, the energy dissipation capacity of the shear wall is higher.

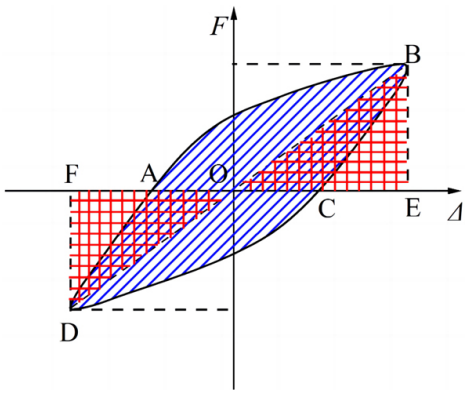

Fig. 8. Illustration for ξ_e

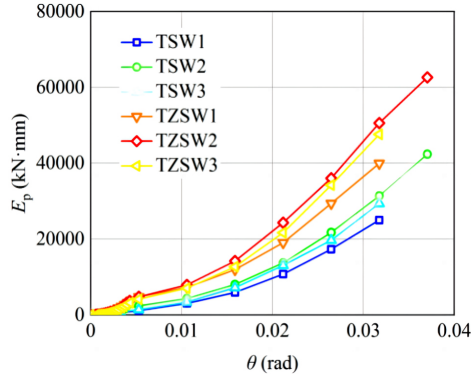

Fig. 9. Accumulated energy dissipation curves

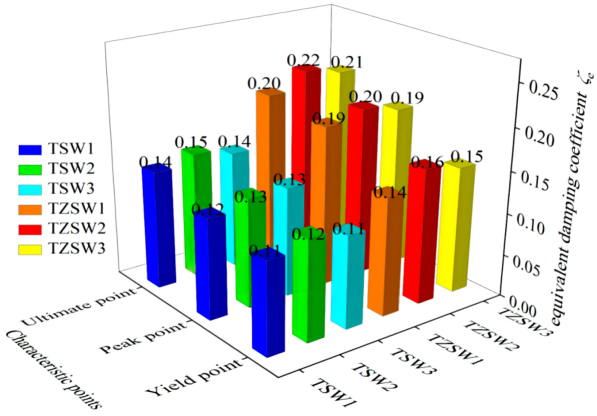

Fig. 10. ξ_e at characteristic points

4. Predicted load carrying capacity

The experimental results show that the six shear wall specimens are mainly flexural failure, which belongs to large eccentric compression. The bearing capacity calculation models of aeolian sand concrete shear walls with CFST columns and aeolian sand concrete shear walls with CFST columns and concealed bracings are shown in Fig. 11a and Fig. 11b, respectively.

According to the test results, the following assumptions are made to establish the bearing capacity calculation model [8, 9]:

1. The cross-section strain conforms to the plane-section assumption.
2. The compressive strength of the concrete in the steel tube is taken as f_c, and the stress of the whole concrete in the boundary steel tube reaches f_c. The concrete stress outside the steel tube in the compression zone is simplified as an equivalent rectangular stress block model with two coefficients α and β [12].
3. The tensile effect of concrete in the tensile zone is not considered.

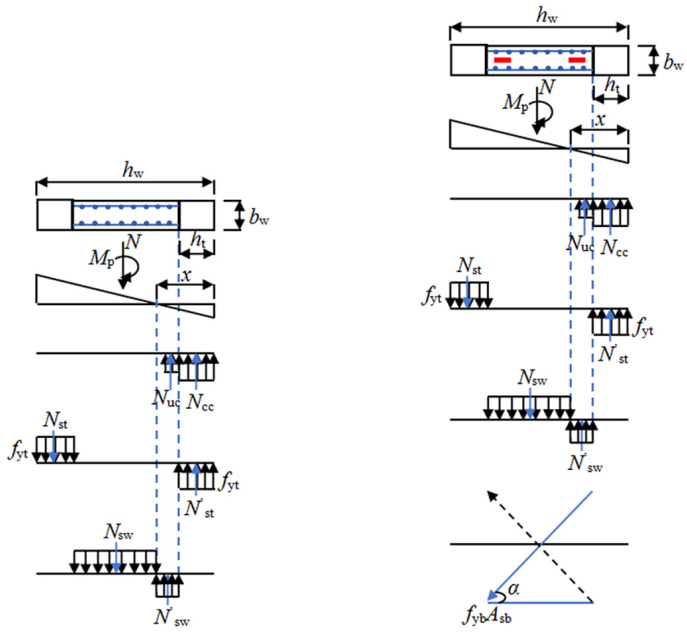

Fig. 11. Model for mechanical calculation: (a) Specimens without concealed bracings, (b) Specimens with concealed bracings

4. The steel bars and steel tubes of all specimens adopt yield strength to simplify the calculation.

The calculation formula of the bearing capacity of the specimen without concealed bracing is as follows:

$$\begin{cases} N_{uc} = \alpha f_c b_w (\beta x - h_t) \\ N_{cc} = \eta f_c A_c \\ N_{st} = N'_{st} = f_{yt} A_{st} \\ N_{sw} = f_{yw} \rho_{sw} b_w (h_w - x - h_t) \\ N'_{sw} = f_{yw} \rho_{sw} b_w (x - h_t) \end{cases} \tag{4.1}$$

$$N = N_{uc} + N_{cc} + N'_{st} + N'_{sw} - N_{st} - N_{sw} \tag{4.2}$$

$$M_p = 0.5 \left[N_{uc}(h_w - \beta x - h_t) + (N_{cc} + 2N_{st})(h_w - h_t) + N_{sw}(x - h_t) + N'_{sw}(h_w - x - h_t) \right] \tag{4.3}$$

$$F_{p,c} = \frac{(M_p - N\Delta_p)}{H} \tag{4.4}$$

where: N_{cc} – resultant force of concrete in the steel tube in the compression zone; N_{uc} – resultant force of aeolian sand concrete in the compression zone of the middle wall; N_{st} – tension of the steel pipe in the tension zone; N_{sw} – resultant force of vertical distributed reinforcement in the tension zone of the intermediate wall; N'_{st} – pressure on the steel tube in the compression

zone; N'_{sw} – vertical distribution of reinforcement force in the compression zone of the middle wall; f_c – axial compressive strength of concrete prism; η – strength improvement coefficient of aeolian sand concrete in steel tube, which is 1.2 [16]; f_{yt} and f_{yw} are the tensile yield strength of steel tube and vertical distributed steel bar, respectively; α and β are the equivalent rectangular stress diagram coefficients, which are obtained according to the stress-strain curve of aeolian sand concrete measured by our research group [16]; x – height of the compression zone; b_w and h_w are the width and height of the cross section of the shear wall, respectively; h_t – external length of the steel tube cross section; A_C – area of concrete in steel tube; A_{st} – cross-sectional area of the steel tube; ρ_{sw} – reinforcement ratio of vertical distributed steel bars; N – axial pressure of the shear wall specimen; M_p – bending moment of the bottom section of the shear wall specimen; $F_{p,c}$ – calculated value of the transverse bearing capacity of the shear wall specimen; Δ_p – lateral displacement measured at the loading point corresponding to the peak load; H – height from the loading point to the upper surface of the bottom beam.

For the specimen with concealed bracing, the bending moment of the section can be found according to the following equation:

$$M_p = 0.5\,[N_{uc}(h_w - \beta x - h_t) + (N_{cc} + 2N_{st})(h_w - h_t) + N_{sw}(x - h_t) + N'_{sw}(h_w - x - h_t) + f_{yb}A_{sb}(h_w - 2a_{sb})\sin\alpha] \tag{4.5}$$

where: f_{yb} – tensile yield strength of the concealed bracing; A_{sb} – cross-sectional area of the concealed bracing; α – dip angle of concealed bracing; a_{sb} – height of the horizontal cross section of the concealed bracing.

In addition to the calculation of the normal section bearing capacity of the six shear wall specimens in this test, this paper also cites four shear walls with CFST columns specimens in the relevant literature [17, 18] to verify the accuracy of the analysis method. The main parameters of 10 shear wall specimens are listed in Table 6. The comparison results of the calculated and experimental values of the normal section bearing capacity of 10 shear wall specimens are shown in Fig. 12. It can be seen from Table 6 that the mean value, standard deviation and variable coefficient of F_c/F_t are 0.98, 0.11 and 0.11, respectively. It can be seen from Fig. 12 that the difference between the calculated value and the experimental value is not greater than

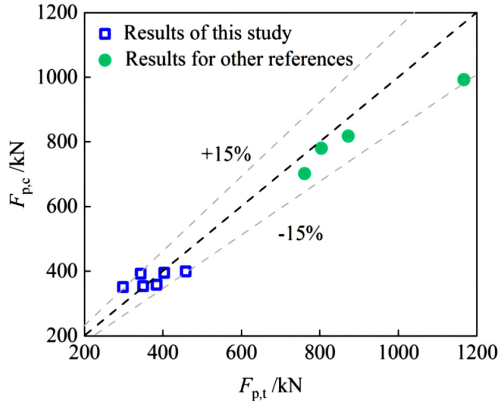

Fig. 12. Comparison between test and calculated results

15%. The calculated values are in good agreement with the experimental values, indicating that the calculation method of the normal section bearing capacity of the shear wall specimen proposed in this section is suitable for the aeolian sand concrete shear walls with CFST columns and the aeolian sand concrete shear walls with CFST columns and concealed bracings.

Table 6. Summary of test for load-carrying capacity

Specimen	f_c **(MPa)**	L **(mm)**	W **(mm)**	H **(mm)**	n	β (%)	**Concealed bracings**	F_c **(kN)**	F_t **(kN)**	
TSW1	27.60	630	100	795	0.2	20	No	350.84	298.29	1.18
TSW2	30.28	630	100	795	0.2	30	No	358.24	383.97	0.93
TSW3	29.21	630	100	795	0.2	40	No	353.75	349.41	1.01
TZSW1	27.60	630	100	795	0.2	20	Yes	392.16	343.28	1.14
TZSW2	30.28	630	100	795	0.2	30	Yes	399.56	458.09	0.87
TZSW3	29.21	630	100	795	0.2	40	Yes	395.07	403.48	0.98
SW1[17]	27.20	925	175	438	0.35	0	No	702.00	760.94	0.92
SW2[17]	27.20	925	175	438	0.65	0	No	780.53	803.60	0.97
SW1[18]	41.60	740	140	590	0.35	0	No	818.20	872.09	0.94
SW2[18]	41.60	740	140	590	0.35	0	Yes	992.88	1167.01	0.85
								Mean value		0.98
								Standard deviation		0.11
								Variable coefficient		0.11

Note: L, W and H are the length, width and height of the shear wall, respectively; n is the axial compression ratio; β is the replacement rate of aeolian sand.

5. Conclusions

Three aeolian sand concrete shear walls with CFST columns and aeolian sand concrete shear walls with CFST columns and concealed bracings were tested to study the influence of concealed bracing on the seismic performance of the proposed shear walls under the same replacement rate of aeolian sand. The conclusion is as below:

1. Under the same replacement rate of aeolian sand, the setting of concealed bracings can significantly improve the load-carrying capacity, ductility, stiffness degradation behavior and energy dissipation capacity of aeolian sand concrete shear walls with CFST columns and concealed bracings.
2. Among the three aeolian sand concrete shear walls with CFST columns and concealed bracings, the specimen with 30% replacement ratio of aeolian sand has better seismic performance.

3. Based on the test, the calculation model of normal section bearing capacity of aeolian sand concrete shear walls with CFST columns and aeolian sand concrete shear walls with CFST columns and concealed bracings is established. The test results are in good agreement with the calculation results.

References

[1] C. Liu, X. Lin, C. Zhu, and H. Liu, "Research progress on application of aeolian sand in concrete", *Journal of Materials Science and Engineering*, vol. 40, no. 4, pp. 695–705, 2022, doi: 10.14136/j.cnki.issn1673-2812.2022.04.024.

[2] H.J. Xue, X.D. Shen and Y.F. Hou, "Mechanical properties and pore characteristics of aeolian sand concrete", *Journal of Drainage and Irrigation Machinery Engineering*, vol. 39, no. 7, pp. 720–726, 2021.

[3] Z.L. Li, "Road performance of aeolian sand concrete", Tianjin, Hebei University of Technology, China, 2021.

[4] X.S. Guo, "Experimental study on the mechanical properties and durability of alkali-excited aeolian sand concrete", Hohhot, Inner Mongolia Agricultural University, China, 2022.

[5] X.H. Zhang, S.J. Xu and S.Y. Li, "Study on shear performance of cold-formed thin-walled steel-paper straw board composite wall with openings", *Archives of Civil Engineering*, vol. 69, no. 1, pp. 571–591, 2023, doi: 10.24425/ace.2023.144189.

[6] J.L. Bian, W.L. Cao, and H. Li, "Experimental study on seismic performance of assembly structure of lightweight CFST frame-embedded steel plate composite wall with different constructions", *Journal of Building Structures*, vol. 42, no. 10, pp. 35–44, 2021, doi: 10.14006/j.jzjgxb.2019.0735.

[7] X. Li, J. Zhang, and W. Cao, "Hysteretic behavior of high-strength concrete shear walls with high-strength steel bars: experimental study and modelling", *Engineering Structures*, vol. 214, 2020, doi: 10.1016/j.engstruct.2020.110600.

[8] J. Zhang, H. Yang, M. Zhang, and X. Liu, "Experimental study on seismic performance of resilient recycled aggregate concrete shear walls", *Structures*, vol. 41, pp. 36–50, 2022, doi: 10.1016/j.istruc.2022.04.096 .

[9] J. Zhang, X. Li, C. Yu, and W. Cao, "Cyclic behavior of high-strength concrete shear walls with high-strength reinforcements and boundary CFST columns", *Journal of Constructional Steel Research*, vol. 182, 2021, doi: 10.1016/j.jcsr.2021.106692.

[10] J.W. Zhang, Y.D. Li, and Y.R. Zhao, "Seismic behavior of prefabricated medium-high strength recycled concrete shear walls with high-strength steel bars in boundary elements", *Journal of Building Structures*, vol. 43, no. 4, pp. 103–113, 2022, doi: 10.14006/j.jzjgxb.2020.0562.

[11] M.K. Deng, Q.Q. Li, and H.B. Liu, "Experimental study on seismic behavior and shear strength calculation of high ductile concrete low-rise shear wall", *Engineering Mechanics*, vol. 37, no. 1, pp. 63–72, 2020, doi: 10.6052/j.issn.1000-4750.2018.05.0290.

[12] GB50010:2010 Code for design for concrete structures. China Machine Press, 2011.

[13] Y. Z. Wang, X. H. Gao, and D. J. Xu, "Experimental analysis on seismic performance of steel reinforced concrete shear wall with different types of steel bracings", *Journal of Civil and Environmental Engineering*, vol. 40, no. 5, pp. 44–53, 2018.

[14] M.K. Deng, J.C. Liu, and Y.X. Zhang, "Investigation on the seismic behavior of steel-plate and high ductile concrete composite low-rise shear walls", *Engineering Mechanics*, vol. 38, no. 3, pp. 40–49, 2021.

[15] JGJ/T 101:2015 Specification for seismic test of buildings. China, 2015.

[16] Z.P. Zhang, "Seismic damage behavior of aeolian sand concrete columns with an inner square steel tube", Hohhot, Inner Mongolia University of Technology, China, 2020.

[17] M. Wang, W.L. Cao, and J.W. Zhang, "Seismic behavior research of composite shear wall with concrete filled steel tube columns for different axial-load ratios", *World Earthquake Engineering*, vol. 24, no. 2, pp. 32–36, 2008.

[18] Y.B. Yang, "Study on seismic experimental and theory of shear wall with concrete filled round steel tube columns and concealed steel trusses", Beijing, Beijing University of Technology, China, 2011.

Received: 2024-05-09, Revised: 2024-07-04